Downloaded from orbit.dtu.dk on: May 12, 2025

DTU Library

Autonomous cryogenic RF receive coil for ^{13}C imaging of rodents at 3 T

Sánchez-Heredia, Juan Diego; Baron, Rafael Antonio; Hansen, Esben Søvsø Szocska; Laustsen, Christoffer; Zhurbenko, Vitaliy; Ardenkjær-Larsen, Jan Henrik

Published in:
Magnetic Resonance in Medicine

Link to article, DOI:
10.1002/mrm.28113

Publication date:
2020

Document Version
Peer reviewed version

Link back to DTU Orbit

Citation (APA):
Sánchez-Heredia, J. D., Baron, R. A., Hansen, E. S. S., Laustsen, C., Zhurbenko, V., & Ardenkjær-Larsen, J. H. (2020). Autonomous cryogenic RF receive coil for ^{13}C imaging of rodents at 3 T. *Magnetic Resonance in Medicine*, *84*, 497–508. https://doi.org/10.1002/mrm.28113

General rights
Copyright and moral rights for the publications made accessible in the public portal are retained by the authors and/or other copyright owners and it is a condition of accessing publications that users recognise and abide by the legal requirements associated with these rights.

- Users may download and print one copy of any publication from the public portal for the purpose of private study or research.
- You may not further distribute the material or use it for any profit-making activity or commercial gain
- You may freely distribute the URL identifying the publication in the public portal

If you believe that this document breaches copyright please contact us providing details, and we will remove access to the work immediately and investigate your claim.

Autonomous Cryogenic RF Receive Coil for 13C Imaging of Rodents at 3T

Journal:	*Magnetic Resonance in Medicine*
Manuscript ID	MRM-19-20209.R1
Wiley - Manuscript type:	Full Paper
Date Submitted by the Author:	15-Oct-2019
Complete List of Authors:	Sánchez-Heredia, Juan Diego; Technical University of Denmark, Department of Electrical Engineering Baron, Rafael; Technical University of Denmark, Department of Health Technology Hansen, Esben; Aarhus University, Laustsen, Christoffer; Aarhus University, MR center Zhurbenko , Vitaliy; Technical University of Denmark, Department of Electrical Engineering Ardenkjær-Larsen, Jan; Technical University of Denmark, Department of Electrical Engineering
Research Type:	RF Coils < Instrumentation < Technical Research
Research Focus:	No specific tissue or organ focus

SCHOLARONE™
Manuscripts

Autonomous Cryogenic RF Receive Coil for ^{13}C Imaging of Rodents at 3T

Juan Diego Sanchez-Heredia[a*], Rafael Baron[a], Esben Søvsø Szocska Hansen[b], Christoffer Laustsen[b], Vitaliy Zhurbenko[a] and Jan Henrik Ardenkjær-Larsen[a,c]

a Department of Health Technology, Technical University of Denmark, Kgs. Lyngby.

b MR Research Centre, Department of Clinical Medicine, Aarhus University, Aarhus.

c GE Healthcare, Denmark

* Correspondence to:

Juan Diego Sanchez-Heredia

Department of Health Technology

Technical University of Denmark, Kgs. Lyngby.

E-mail: jdsanch@dtu.dk

For Peer Review

Keywords: Cryogenic RF coil; SNR; ^{13}C MRI; hyperpolarization

Word count: 4555 words

ABSTRACT

PURPOSE: To develop an autonomous, in-bore, MR compatible cryostat cooled with liquid nitrogen that provide full day operation. To demonstrate that the theoretical signal-to-noise benefit can be achieved for ^{13}C imaging at 3 T (32.13 MHz).

METHODS: The cryogenic setup uses a vacuum insulated fiberglass cryostat, which indirectly cools a cold-finger where the RF coil is attached. The cryostat is evacuated before use and has a reservoir of liquid nitrogen for full day operation. A 30 by 40 mm^2 copper coil is mounted inside the cryostat with a 3 mm distance to the sample. Two examples of in-vivo experiments of rat brain metabolism after a hyperpolarized [1-^{13}C]pyruvate injection are reported.

RESULTS: A coil Q-factor ratio of Q_{88K}/Q_{290K} = 550/280 is obtained, and the theoretical SNR enhancement is verified with MR measurements. We achieved a coil temperature of 88 K and a preamplifier temperature of 77 K. A 2-fold overall SNR enhancement is achieved, compared to the best case at room temperature. The thermal performance of the coil is adequate for in-vivo experiments, with an autonomy of 5 h consuming 6 L of LN_2, extendable to over 12 h by LN_2 refilling.

CONCLUSION: Cryogenic surface coils can be highly beneficial for ^{13}C imaging, provided that the coil-to-sample distance remains short. An autonomous, in-bore cryostat is developed that achieves the theoretical improvement in signal-to-noise ratio.

For Peer Review

INTRODUCTION

Cooling of RF coils has been an attractive method to improve SNR in MRI since its early days, with the first prototypes dating back to the second half of the 80´s (1), including the first experiments with cryogenically cooled human coils (2). Prototypes of superconducting coils were already developed during the early 90´s (3,4). For small samples, such as those used in MR microscopy, cryogenic coils have proven to be very useful to improve image quality, where over 10-fold SNR enhancements have been reported over room temperature coils (5–7). Since approx. a decade, a commercial alternative has been made available by Bruker (Billerica, Massachusetts, USA) for small animal imaging, showing the first indications of the potential of this technology. This solution provides a cooling of the coil to 30 K through a helium closed cycle system, which requires a cryocooler connected to the coil and close to the MR scanner. Additionally, a strong heat source is applied to the animal position in order to create a very high thermal gradient (>220 °C), over a coil-to-sample distance of 1 mm in a stable manner. The SNR-gain over room temperature coils obtained is highly dependent on the target organ and frequency, with reported enhancements of 2-2.2 for mouse brain at 200 MHz (8), 2.4-2.5 for mouse brain at 400 MHz (9), 3-5 for mouse heart at 400 MHz (10) and 3-3.5 for mouse brain at 100 MHz (11).

However, the high economic cost of such commercial alternatives, calls for further development of this technique in order to make it widespread to many other applications and nuclei. Some simplified options using liquid nitrogen (LN_2) as a coolant instead of a dedicated cryocooler, have already been reported for small surface coils aimed for animal MRI. For example Elabyad et al. reported a 2.7-fold SNR gain (18.68 MHz) for rat heart, using a cryostat where the coil is directly immersed in LN_2, and solid insulation (5 mm thick) is placed around the coil (12). A more sophisticated approach, including a vacuum layer for thermal insulation (1.5 mm thick) was suggested by Hu et al. in (13), where an 1.6-fold SNR gain was obtained for mouse brain at 3 T. In this case, however, a constant connection to a vacuum pump was needed in order to maintain the thermal insulation during the MR experiments. A cryostat with an autonomy of 5 h has been reported in (7), cooling a transmit-receive HTS coil inductively coupled to an external loop. However, the practical benefit of cryogenic coils for in-vivo imaging of larger objects, clinically in particular, has been limited due to increased coil-to-sample distance, and the potential lack of robustness and flexibility introduced by the cryostat. In this work we aim to achieve a LN_2-based cryogenically cooled coil setup where no additional hardware is needed inside the scanner room, and where the coil is fully compatible with the animal cradles routinely used with room temperature coils. This specifically means that we avoid the use of a cryocooler, a vacuum connection and any additional heating source (due to the cryogenic coil) during the MR experiments. The setup is also designed in a modular way, such that the coil and preamplifier can be easily replaced, in order to provide flexibility to perform experiments with different nuclei and/or coil geometries. The total cost of the whole setup is about an order of magnitude lower

For Peer Review

than the commercial alternatives, due to the absence of a cryocooler (and the running and maintenance cost that it involves). Additionally, the cost of any additional replaceable coil is below 600 USD. The whole setup is designed in such a way, that scaling it to bigger FOV (with the use of phased arrays) would be relatively straight forward, and therefore has the potential of being extended to clinical applications. This includes specifically the use of receive-only coils, interfaced through ohmic connections, where active detuning from the transmitter can also be implemented and the whole receive chain is cooled. The aim of the coil setup presented here is hyperpolarized ^{13}C MRSI at 3 T (32.13 MHz) (14), which is a particularly interesting case for cryogenic coils, since the magnetization of the injected compound is not recoverable, and therefore time averaging is not an option to increase image quality. Additionally, hyperpolarization experiments are especially sensitive to flip angle inhomogeneities, since the magnetization of the injected compound can be reduced considerably if it passes through an area with very high B_1^+. For this reason, the coil proposed here is used as receive-only (unlike most of the reported studies using the commercial CryoProbes), in order to allow the B_1^+ to be generated with an external (more homogenous) coil.

In our design, both the coil and the preamplifier are indirectly cooled (through cold-fingers) to 88 K and 77 K respectively. A cryostat was specifically developed for this purpose, made with MRI transparent materials, and therefore not disturbing the RF performance of the coil. The system was designed so that it can be cooled in less than an hour, and then used for a whole scan session (of over 12 h). During that time, no additional vacuum connection or heat source are needed inside the MRI scanner room, besides of the standard warm-air flow used routinely for small animal imaging. The final coil-to-sample distance of this setup is 3 mm.

The coil used is a 30x40 mm^2 octagonal copper loop, which serves as a multi-purpose surface coil for rodents. A matching network nearly optimal for cryogenic coils (previously reported in ((15,16)), is used in order to de-tune the receive coil during transmission. This implementation ultimately allows us to obtain an unloaded Q-factor (Q_{UN}) of 550 when the coil is stably cooled to 88 K, which is higher than other LN_2 cooled copper surface coil reported to this day (Q_{UN} = 450 in (12), Q_{UN} = 210 in (13)), and even higher than the commercially available option (Q_{UN} = 353 in (11)) despite of its lower temperature.

The theoretically predicted SNR enhancement is confirmed with MR experiments, comparing to an identical setup at room temperature (with a similar coil-to-sample distance), and a more fair comparison to a similar coil placed as close as possible to the sample, where a nearly 2-fold SNR gain is obtained. Additionally, the setup has been successfully used to obtain ^{13}C metabolic images of the healthy rat brain in-vivo with hyperpolarized [1-^{13}C]pyruvate, a particularly low SNR case (17), (18).

For Peer Review

THEORY

In traditional ^{1}H MRI, the contribution of noise coming from the object to image is often dominating. As either the physical dimensions or the detection frequency of the imaging experiments are reduced, the contribution of the thermal noise in the conductor of the coil and electronics becomes more relevant, ultimately prevailing (19). The expected SNR enhancement when cooling a receive coil (including the first preamplifier), is then defined by the coil-to-sample noise ratio and equivalent noise temperature of the amplifier. This can be written in terms of Q-factors, for a coil matched to 50 Ohms, as (20):

$$SNR_{GAIN} = \frac{SNR_{LT}}{SNR_{RT}} = \sqrt{\frac{n_{cRT}^2 + n_{sRT}^2 + n_{pRT}^2}{n_{cLT}^2 + n_{sRT}^2 + n_{pLT}^2}} = \sqrt{\frac{Q_{LO\,LT} \cdot \left[\frac{T_{RT} \cdot Q_{LO\,RT}}{Q_{UN\,RT}} + \frac{T_{RT} \cdot Q_{LO\,RT}}{Q_{S\,RT}} + T_{pRT}\right]}{Q_{LO\,RT} \cdot \left[\frac{T_{LT} \cdot Q_{LO\,LT}}{Q_{UN\,LT}} + \frac{T_{RT} \cdot Q_{LO\,LT}}{Q_{S\,LT}} + T_{pLT}\right]}} \quad (1)$$

Where: n_C^2 = coil noise power, n_S^2 = sample noise power, n_P^2 = preamplifier noise power, T_{RT} = room temperature, T_{LT} = low temperature, T_P = preamplifier equivalent noise temperature, $Q_{UN\,RT}$ = Q at room temperature without sample, $Q_{LO\,RT}$ = Q at room temperature with sample, $Q_{UN\,LT}$ = Q at low temperature without sample, $Q_{LO\,LT}$ = Q at low temperature with sample. Note that the Q of the sample does not change when cooling the coil, and therefore $Q_{S\,RT} = Q_{S\,LT}$, which can be calculated indistinctively at RT or LT from the relation $Q_S = (Q_L^{-1} - Q_{UN}^{-1})^{-1}$.

For copper coils, a large reduction (8-fold) of the resistivity is obtained already at temperatures around the LN_2 boiling point (77 [K]) compared to room temperature (21). In the present work, a copper coil cooled with LN_2 was chosen, in order to avoid the added complexity and cost of a liquid helium cryocooler and HTS materials. Additionally, the solution proposed here can be potentially scaled to cover much bigger FOVs, with the prospect of eventually extending the design to human applications.

METHODS

Cryostat Design

An RF transparent cryostat was specifically developed, made mostly of fiber reinforced plastic (FRP). The cryostat consists of two main parts: an LN_2 reservoir, and a horizontal vacuum insulated vessel with an inner bore where the animal can be placed. Reservoir and vessel are connected through a 10 mm diameter pipe, which allows the LN_2 to flow from the reservoir to the vessel, and fill it. Both the reservoir and the vessel have a geometric volume of 4 L each, allowing a maximum of 8 L of LN_2 in the cryostat. Additionally, a bag of activated charcoal and a bag of sodium aluminum silicate (approx. 100 mL of each) are placed inside the cryostat, in good thermal contact

For Peer Review

with the LN_2 vessel. These molecular sieves, absorb (when they are cold) small molecules that could enter the vacuum volume or outgas, therefore extending vacuum holding time of the cryostat. A schematic of the cryostat is shown in Fig. 1.

A separate ceramic (Al_2O_3) disk (AdValue Tech, AZ, USA) whose outer diameter matches the inner diameter of the vessel acts as a cold-finger, where the RF coil(s) can be attached. Al_2O_3 (99.6 % purity) was chosen as the material for the cold-finger due to its relatively low cost, and good thermal conductivity around the LN_2 temperature, with its optimal of approx. 1000 [W/mK] happening in the region between 80 K to 90 K (22).

Besides the vacuum jacket for thermal insulation, additional multi-layer insulation (MLI) was installed, to reduce radiation heat losses. An MLI with 5 layers of aluminized mylar was used around the whole LN_2 vessel, except for the part closer to the RF coil position, where non-metallic (polyimide) MLI was used, in order to avoid eddy currents. With this solution, the more efficient metallic MLI was maintained in all the parts of the cryostat where it does not disturb the receive coil, and replaced by polyimide only at the exact position of the coil. The fabricated cryostat (ILK Gmbh, Dresden, Germany) is shown in Fig. 2a.

To evaluate the thermal performance of the cryostat, a temperature sensor (C220 Pt100, Heraeus Gmbh, Hanau, Germany) was attached to the surface of the cold-finger. The temperature outside the cryostat (at the animal position) was monitored simultaneously. The temperatures inside and outside the cryostat were evaluated under two different situations: a) no heat applied externally to the inner bore, and b) warm air (50 °C) applied to the inner bore. The amount of LN_2 consumed during the experiment was 6 L. The use of a stream of warm air to keep the room temperature at the animal position, instead of a more efficient animal coat of warm liquid, was used in this case solely because this was the standard method used at the facility where the in-vivo experiments were performed.

The cooling procedure of the cryostat was done in steps as follows:

1- Cryostat vacuum build-up, reaching a pressure below 10^{-3} mbar (prior to cooling).
2- Start of the cooling process: filling the cryostat with 6 L of LN_2.
3- Cooling transient period: after 45 min, the cryostat can be disconnected from the vacuum pump.
4- The cryogenic RF coil is now cold and temperature is stable.

Finally, in order to characterize the operational performance of the cryogenic setup, several parameters were monitored during a whole usage cycle of 20 h (temperature at the sample position, cryostat pressure, coil Q-factor, and resonance frequency), which included a LN_2 refill (4 L), to demonstrate the long-term performance.

For Peer Review

RF Coil

An octagonal 40x30 mm^2 geometry was chosen for the RF coil, in order to get good coverage of the whole rat brain (typically as deep as 15 mm). This coil size is also suitable as a multipurpose small animal surface coil. The RF coil was made out of flat (1.2 mm thick) copper, to maximize the contact surface with the cold finger and therefore increase the thermal transfer between them. The inductance of such coil geometry (estimated from simulation) is about 40 [nH]. For a coil of such a small size, and for the low frequency used here, the selection of a high-Q tuning capacitor is critical. A mica fixed capacitor (MCM01, Cornell Dubilier, SA, USA) of 620 pF was chosen due to its good performance at low temperatures (both electrically and mechanically). For fine tuning, a trimmer (80H85, Johanson Technology, Camarillo, CA, USA) was added in parallel. Previous work has shown that stacking several capacitors in parallel can lead to a reduction in the equivalent series resistance (ESR) of the capacitor (23). For the capacitor series (and frequency of operation) used here, this point could not be confirmed experimentally, and therefore we chose to tune with only one fixed tuning capacitor in order to minimize soldering connections and improve the thermal transfer to the capacitor.

The rest of the matching network used (as described in (16)) was completed using standard SMD capacitors (Johanson Technology, Camarillo, CA, USA), inductors (Coilcraft, Cary, IL, USA) and PIN diodes (MA4P7470F-1072T, MACOM, Lowell, MA, USA). Fast switching diodes (UMX9989AP, Microsemi, Aliso Viejo, CA, USA) were used for the preamplifier input protection.

The coil was then attached to the cold-finger using thermally conductive epoxy (STYCAST 2850, Emerson & Cuming, MA, USA), with a thermal conductivity of 1.25 [W/mK]. The cold-finger, with the RF coil attached, is shown in Fig. 2b.

A preamplifier (WMA32C, WantCom, Chanhassen, USA) was connected directly to the coil, and placed in direct contact to the LN_2 vessel, ensuring good thermal contact to it. The preamplifier, which was not rated for cryogenic temperatures, was characterized both at room temperature and at 77 K. Gain, Noise Figure (NF) and noise temperature were measured using a spectrum analyzer with noise measurement capability (PSA E4440A, Keysight, CA, USA). Also its current consumption was monitored.

The RF coil (including all the tuning-matching-decoupling circuitry) was characterized in terms of its Q-factor, both without the sample (unloaded) and under different sample loading conditions. The first loading condition used was using a spherical phantom with 38 mm diameter containing a 1.0 M solution of ^{13}C-bicarbonate sodium salt (85 mg/mL) in water. The measurements were repeated at room temperature, and after cooling. Two different measurements of the unloaded coil were done at low temperature: one with the coil mounted in the cryostat, and another one with the coil immersed in LN_2 (to be used as a reference).

For Peer Review

Due to the high ^{13}C-bicarbonate concentration, this phantom has higher conductivity than the nominal tissue values at 32 MHz (24), and is used here as worst case scenario of sample loading for rat head. A characterization of the phantom loading, compared to the in-vivo sample loading caused by a female Wistar rat (250 g) was also measured for two imaging cases: head and abdomen. These results are provided as supplementary information to this manuscript in Supporting Information Figure S1 and Supporting Information Table S1.

The Q-factor was measured using a double loop probe (decoupled more than 85 dB through overlap). The Q-factor was then calculated as the resonance frequency divided by the 3 dB bandwidth of the S_{12} response of the double-loop probe, when loosely coupled to the evaluated coil (25).

Phantom Validation

The SNR enhancement of the coil over its room temperature counterpart was evaluated on the same ^{13}C labelled phantom (described in the previous section), due to the more repeatable ^{13}C signal levels in-vitro, compared to the in-vivo conditions where the signal polarization is different in different experiments (making it extremely difficult to accurately characterize SNR difference due to the coil).

The performance of the cryogenic coil was validated with MR measurements, first by performing a phantom characterization. Using the same cooling procedure described above, MR experiments were performed on the same ^{13}C-enriched bicarbonate phantom described in the previous section. A CSI sequence was used, with 16x16 acquired points, TR=75ms and FOV= 80 mm x 80 mm x 10 mm.

The SNR was calculated from the obtained spectra (26) as the maximum of the detected bicarbonate signal in each voxel, divided by the variance of a noise ROI. In order to validate the ideal SNR enhancement expected from the measured Q-factors, the measurements were repeated using an identical surface coil at room temperature. Two measurements with the room temperature surface coil were made: one with a coil-to-sample distance of 3 mm (to replicate the setup of the cryogenic coil), and one with a coil-to-sample distance of 0 mm (to replicate a real-use condition). Finally, a measurement using a volume birdcage coil was done as reference (27), in order to determine what is the maximum depth where the use of the cryogenic surface coil is beneficial.

A separate ^{13}C transmit coil of the clamshell type was used to produce the B_1^+. The coil, similar to the one described in (28,29), has 400 mm of diameter and 300 mm of length.

In-vivo Hyperpolarized ^{13}C Experiments

The compatibility of the proposed coil setup with in-vivo experimental conditions was evaluated. For this purpose, two female Wistar rats (250 g) were used for the in-vivo experiments, and their vital signs were controlled over the whole scanning session in order to detect any adversity due to the cryogenic coil.

For Peer Review

Before the MR protocol, the animals were housed with ad libitum access to standard rodent diet and tap water in a 12/12 day/night cycle with a temperature of 21±2 °C and humidity 55±5%. All experiments were performed in accordance with Danish and international legislation, regulations and guidelines and were approved by the Danish Animal Experiments Inspectorate under the Danish Veterinary and Food Administration (license no. 2014-15-0201-00327). Anesthesia was maintained throughout the experiment with Sevoflurane (3% in 2 L/min air). Anatomical ^{1}H reference scans were performed using the body coil for transmission and reception. The hyperpolarized [1-^{13}C]pyruvate experiment was performed in either the axial or coronal plane using a spectral-spatial spiral ^{13}C imaging sequence (30) with a field of view of 80 mm and slice thickness of 16 mm. The individual metabolite frequencies (and flip angle) for lactate(90˚), pyruvate(8˚), bicarbonate(90˚), pyruvate(8˚), alanine(90˚), pyruvate(8˚) were cycled repeatedly with an effective TR of 500 ms. [1-^{13}C]pyruvate was prepared and hyperpolarized to a reproducible polarization of above 40% in a clinical ready polarizer (31), similar to previous reports (32). The experimental setup is shown in Fig. 3.

RESULTS

Q-factors

Table I shows the measured Q-factors comparing the performance of the cryogenic coil at room temperature and cold. The Q-factor difference between the case where the coil is immersed in LN_2 (77 K) and cooled inside the cryostat (88 K) is 7% (590 vs. 550). The Q-factor reduction when loading the coil with a phantom (at low temperature) is about 22%, which shows that even at low temperature, the thermal noise of the coil dominates over the sample noise for such a small coil at the frequency of 32 MHz.

The Q-factor increase obtained when cooling is nearly a factor of 2 (Q_{88K}/Q_{290K} = 550/280), which agrees well with previously reported cryogenic copper coils cooled to similar temperatures (12,16,33). While copper resistivity is reduced 8 times when cooling from 290 K to 77 K (21), the reduction of resistance of a wire loop is only the square root of that ($\sqrt{8}$ = 2.82) due to the skin effect. However, for small coils (with low inductance), the losses on the tuning capacitor contribute significantly (often predominantly) to the total loss (16). That explains why the Q-factor improves only a factor of 2, instead of 2.82.

From the measured Q-factors, the expected SNR enhancement from the cooling can be estimated as follows, based on the notation given in Eq. 1:

For Peer Review

$$\frac{SNR_{88K}}{SNR_{290K}} = \sqrt{\frac{Q_{LO\,LT}\cdot\left[\frac{T_{RT}\cdot Q_{LO\,RT}}{Q_{UN\,RT}}+\frac{T_{RT}\cdot Q_{LO\,RT}}{Q_{S\,RT}}+T_{pRT}\right]}{Q_{LO\,RT}\cdot\left[\frac{T_{LT}\cdot Q_{LO\,LT}}{Q_{UN\,LT}}+\frac{T_{RT}\cdot Q_{LO\,LT}}{Q_{S\,LT}}+T_{pLT}\right]}} = \sqrt{\frac{430\cdot[256+36+51]}{245\cdot[69+63+17]}} = 2.01 \quad (2)$$

Table II shows the measured performance of the preamplifier connected to the coil, both at room temperature and when cold. The measured noise temperature improves from 51 K to 17 K, with the gain being reduced by 5.7 dB at low temperature. The reduction in gain is consistent with a lower current consumption. The measured noise temperature at 77 K agrees well with previously reported data for HEMT cryogenic low-noise amplifiers (34).

Thermal Performance

Several parameters related to the thermal stability of the cryogenic coil setup are shown in Fig. 4 over a whole use cycle (up to 20 h). The upper plot shows the measured temperature at the animal position (inner bore of the cryostat, and closest point to the RF coil). There, it is seen that the thermal insulation provided by the vacuum layer and MLI is sufficient to keep a temperature above 8 °C. It is important to notice that for this measurement, no external warm air was applied, so this represents a worst-case scenario.

The second measurement in Fig. 4 shows the pressure inside the evacuated volume of the cryostat. After the first 45 min of cooling, the cryostat is disconnected from the vacuum pump, and the cold molecular sieves then maintain the vacuum. The measured results show that the threshold of thermal insulation (10^{-3} [mbar]) is reached about 12 h (for the basic use) and 15 h (for the extended use, with an LN_2 refill) after disconnecting the coil from the vacuum pump. This shows the good performance of the molecular sieves to keep vacuum low, when the whole setup is not connected to a vacuum pump (as it is the case during MR scanning). Note that the scale do not go below 10^{-4} [mbar] since the accuracy of the pressure gauge used was not sufficient below that level.

The last two measurements of Fig. 4 show the measured Q-factor and resonance frequency over time. The measured results show that after 45 min of cooling, the cryogenic coil reaches a stable usable regime for the next 5 h in the basic use. The resonance frequency varies only minimally (within 10 kHz) over that time. This result confirms the stable cooling performance of the setup, even after a few hours of use, when the cryostat is only partially filled with LN_2. The performance with an additional refill of LN_2 (4 extra liters added after 4 hours) is also shown in dotted lines, showing a stability close to 10 h.

Additionally, in Fig. 5, the temperature of both the RF coil and the animal position is shown when external warm air (at 50 °C) was applied. The temperature was monitored for two hours, where the warm air was applied for 5 min from minute 70 to 75, and later for a longer period of 50 min (from minute 100 to 150). It can be appreciated

For Peer Review

that the application of warm air results in minor increase in temperature of the coil (0.6 K), while is sufficient to keep the animal chamber at room temperature. Note that warm air is routinely applied in any case for in-vivo experiments with anesthetized rats, so its use with the cryogenic coil does not involve the addition of any extra equipment.

Based on this results, it can be defined a standard use cycle of the cryogenic coil as it follows:

- Cooling: the cryostat is filled with 6 L of LN_2. For the next 45 min, the cryostat is kept connected to the vacuum pump until the RF coil reaches its stable working temperature.
- Basic Use: after the cooling phase, the cryogenic coil is now ready to be used for the next 5 h.
- Extended Use: over this period (from hour 5 to hour 15, from the cooling start), the usage time of the coil can be extended by adding extra LN_2 to the cryostat. This can be done, since the pressure inside is still below 10^{-3} [mbar], and therefore can provide thermal insulation.
- Warm-Up: 12 h after the cooling start, the pressure inside the cryostat is not low enough to provide thermal insulation, and the cryostat needs to be re-connected to the vacuum pump.

MR Performance: Phantom Experiments

The measured SNR of the cryogenic coil is shown in Fig. 6.c), compared to the results obtained for the reference coils at room temperature previously described.

Fig. 6.a) shows the SNR measured with a surface coil identical to the cryogenic coil in size and shape and placed at the same distance to the phantom (3 mm), but at room temperature. The comparison between them shows an SNR enhancement of more than 2-fold for the cryogenic coil close to the phantom surface, which agrees well with the expected improvement (calculated from the measured Q-factors). A more relevant comparison is given in Fig 6.b), where the room temperature surface coil is placed as close as possible to the phantom (coil-to-sample distance = 0 mm). Even then, it is appreciated that the cryogenic coil has superior performance, with an almost 2-fold SNR enhancement close to the phantom surface.

Finally, the last figure 6.d) shows the performance of an 80 mm bore volume coil (of the birdcage type). The comparison to the cryogenic coil shows a 5-fold SNR enhancement at the surface, with the SNR being better for the cryogenic coil up to a depth of 20 mm within the phantom. This result shows that the cryogenic coil is beneficial for imaging of organs placed as deep as 20 mm, but not deeper.

For Peer Review

MR Performance: In-vivo Hyperpolarized ^{13}C Brain Imaging

The ^{13}C metabolic imaging results of the two rat brain experiments, obtained after a hyperpolarized [1-^{13}C]pyruvate injection, are shown in Fig. 7 and Fig. 8. The acquisition was performed over 60 s (with a time interval of 3 s) but, for the sake of simplicity, it is presented here as four averaged time periods of 15 s each. The four metabolites acquired (pyruvate, lactate, bicarbonate, alanine) are shown in different columns from left to right, overlaid with an anatomical image of the rat head, acquired over an identical FOV.

Fig. 7 shows metabolic maps clearly distinct for the different metabolites, and consistent with the morphology of the anatomical image. Additionally, high amounts of alanine are detected in deep parts of the head (especially at the beginning of the experiment), which indicates that the cryogenic coil has sufficient penetration to cover the entire rat head. More interestingly, high amounts of pyruvate and lactate are detected in the brain region, with lactate still clearly visible in the last part of the experiment. This result confirms the high sensitivity of the cryogenic coil, capable of detecting hyperpolarized signal 60 s after the beginning of the experiment. The metabolic results shown in Fig. 8 for the second experiment (obtained on a different day, and with a different animal), are consistent with the first experiment.

Both experimental sessions lasted over 5 h, where the animal was inside the cryogenic coil continuously over that time. No adverse effects on the body temperature or vital signs of any of the animals were observed over the whole scanning session, with the external warm air applied being sufficient to keep the body temperature of the anesthetized animals. From a coil point of view, several calibration measurements were performed before the pyruvate injection, with the coil being stable over the whole experimental session.

DISCUSSION

In this study we demonstrate an MR compatible cryostat design that allows for a whole scanning session (of over 12 h), without the need of any external device connected to the coil during operation.

We use this setup to demonstrate that a copper coil cooled to 88 K, can be highly beneficial for hyperpolarized ^{13}C experiments of small animals. A 2.0-foldSNR enhancement is reported for phantom MR experiments, compared to a similar coil at room temperature and at a similar distance, which agrees well with the expected enhancement obtained from the measured Q-factors (Q_{88K}/Q_{290K} = 550/280). The measured enhancement compared to the same coil, placed as close as possible to the sample, slightly below 2-fold. This result shows that the cryogenic coil can be beneficial for ^{13}C rat experiments at 3 T. A commercial preamplifier is placed directly on the coil, and also cooled, with the noise temperature being reduced from 51 K at 290 K to 17 K at 77 K.

For Peer Review

The 1.5 mm vacuum layer, together with a non-metallic MLI made of polyimide (to reduce radiation heat losses), proves to be sufficient thermal insulation to place a small animal inside the coil bore with the only aid of a standard warm air (50 °C) stream for several hours. This leads to a final coil-to-sample distance of 3 mm. The cryostat is mainly made of MRI transparent materials, which increases the difficulty of obtaining good vacuum performance over a long period of time. To solve this problem, we include inside the vacuum chamber of the cryostat two different molecular sieves (activated charcoal and sodium aluminum silicate), which extend the vacuum hold time of the cryostat when is cold. This allows an autonomy of over 12 h (depending on the amount of LN_2 used), where the cryostat can be disconnected from the external vacuum pump. This modification simplifies greatly the MR experimental setup, since no vacuum connection is needed inside the MR scanner room, unlike other solutions previously proposed (13).

The cooling performance of the coil is also reported with the coil being fully cold and stable 45 min after the beginning of the cooling process, which is similar to LN_2 based cryogenic coils previously reported. We cannot compare this figure to the commercially available CryoProbe, since none of the studies reported with it mentions this important parameter. The closest figure publicly available, is the reported cooling time for NMR CryoProbes, with a similar design (but smaller size) than the MRI CryoProbe, where the cooling time is said to take up to 4 h.

For most of the experiments reported here, an amount of 6 l of LN_2 was used, which provides 5 h of usability. After that time, the LN_2 deposit can be re-filled to extend the usability over 12 h. Two very important parameters for the usability of a cryogenic coil are the repeatability and robustness of the coil, after the cooling process. For all the characterization and MR measurements reported throughout this work, more than 20 cooling cycles have been performed, with the coil showing a very repeatable performance in terms of Q-factor and resonance frequency. The very low sample loading at the frequency of ^{13}C at 3 T (32.13 MHz) allows to have a fixed frequency on the coil, with no tuning and matching needed. This allows the use of a matching-detuning network optimized for cryogenic coils at low frequency (16), which ultimately provides an unloaded Q-factor of 550, which is the highest reported to this day for a cryogenic copper surface coil.

The suitability of the proposed cryogenic coil setup with in-vivo experimental conditions has been successfully demonstrated, and two different experiments of ^{13}C hyperpolarized metabolic imaging (performed in healthy rats) are reported. The imaging case chosen for this initial experience was rat brain metabolic imaging, which is a particularly challenging modality due to the reported low level of permeability of the brain blood barrier in anesthetized animals (18). The initial results show clear metabolic maps, consistent with the brain anatomy. While the experiments presented here on healthy animals are not sufficient to draw biological conclusions at this point, the results show a first indication of the potential of cryogenic surface coils for ^{13}C metabolic imaging at 3T. This is especially interesting for the future development of dedicated cryogenic coil arrays (35), which would

For Peer Review

allow to combine the benefits of cryogenic cooling with the unique benefits of parallel imaging in hyperpolarized experiments (28,36).

CONCLUSION

Cryogenic surface coils can provide a significant SNR improvement for ^{13}C MRI at 3T of small animals. In this study, a cryogenic copper coil setup is reported with a coil-to-sample distance of 3 mm, which provides nearly a 2-fold SNR improvement compared to a similar coil at room temperature (coil-to-sample of 0 mm), measured on a phantom. The coil used has an octagonal shape (30 mm wide, 40 mm long), an unloaded Q-factor of 550 is achieved when cooling to 88 K. We report excellent thermal stability of the coil for 5 h (for 6 L of LN_2), which can be extended over 12 h by adding more LN_2. The coil is designed such that is fully autonomous, and no additional hardware is needed during operation, which simplifies greatly its use for MR experimentation.

The design is very affordable, and therefore economically attractive for labs where several coil geometries and/or nuclei are of interest (compared to the cost of acquiring several commercial cryogenic coils).

The setup is proven to be fully compatible with in-vivo experiments, and the enhanced sensitivity of the cryogenic coil allows improved metabolic imaging of the rat brain. The SNR enhancement provided by the cryogenic coil, opens the possibility to new metabolic experiments with small animals, where the sensitivity would usually be too low for standard coils.

ACKNOWLEDGMENTS

This work has been partly funded by the Danish Council for Independent Research (DFF – 4005-00531) and the Danish National Research Foundation (DNRF124).

REFERENCES

1. Styles P. A High-Resolution NMR Probe in which the Coil and Preamplifier are Cooled with Liquid-Helium. J. Magn. Reson. 1984;60.

2. Hall AS, Barnard B, McArthur P, Gilderdale DJ, Young IR, Bydder GM. Investigation of a whole-body receiver coil operating at liquid nitrogen temperatures. Magn. Reson. Med. 1988;7:230–235 doi: 10.1002/mrm.1910070211.

3. Black R, Early T, Roemer P, et al. A high-temperature superconducting receiver for nuclear magnetic resonance microscopy. Science (80-.). 1993;259:793–795 doi: 10.1126/science.8430331.

For Peer Review

4. Withers RS, Cole BF, Johansson M, Avenue WM. Thin-film hts probe coils for magnetic-resonance imaging. IEEE Trans. Appl. Supercond. 1993;3:2450–2453.

5. Hurlston SE, Brey WW, Suddarth SA, Johnson GA. A high-temperature superconducting Helmholtz probe for microscopy at 9.4 T. Magn. Reson. Med. 1999;41:1032–1038 doi: 10.1002/(SICI)1522-2594(199905)41:5<1032::AID-MRM23>3.0.CO;2-X.

6. Koo C, Godley RF, Park J, McDougall MP, Wright SM, Han A. A magnetic resonance (MR) microscopy system using a microfluidically cryo-cooled planar coil. Lab Chip 2011;11:2197 doi: 10.1039/c1lc20056a.

7. Poirier-Quinot M, Ginefri J-C, Girard O, Robert P, Darrasse L. Performance of a miniature high-temperature superconducting (HTS) surface coil for in vivo microimaging of the mouse in a standard 1.5T clinical whole-body scanner. Magn. Reson. Med. 2008;60:917–927 doi: 10.1002/mrm.21605.

8. Ratering D, Baltes C, Nordmeyer-Massner J, Marek D, Rudin M. Performance of a 200-MHz cryogenic RF probe designed for MRI and MRS of the murine brain. Magn. Reson. Med. 2008;59:1440–1447 doi: 10.1002/mrm.21629.

9. Baltes C, Radzwill N, Bosshard S, Marek D, Rudin M. Micro MRI of the mouse brain using a novel 400 MHz cryogenic quadrature RF probe. NMR Biomed. 2009;22:834–842 doi: 10.1002/nbm.1396.

10. Wagenhaus B, Pohlmann A, Dieringer MA, et al. Functional and Morphological Cardiac Magnetic Resonance Imaging of Mice Using a Cryogenic Quadrature Radiofrequency Coil Morishita R, editor. PLoS One 2012;7:e42383 doi: 10.1371/journal.pone.0042383.

11. Sack M, Wetterling F, Sartorius A, Ende G, Weber-fahr W. Signal-to-noise ratio of a mouse brain 13 C CryoProbe ™ system in comparison with room temperature coils : spectroscopic phantom and in vivo results. NMR Biomed. 2014:709–715 doi: 10.1002/nbm.3110.

12. Elabyad IA, Kalayciyan R, Shanbhag NC, Schad LR. First In Vivo Potassium-39 K) MRI at 9.4 T Using Conventional Copper Radio Frequency Surface Coil Cooled to 77 K. IEEE Trans. Biomed. Eng. 2014;61:334–345 doi: 10.1109/TBME.2013.2294277.

13. Hu B, Varma G, Randell C, Keevil SF, Schaeffter T, Glover P. A Novel Receive-Only Liquid Nitrogen ($\hbox{LN}_{2}$)-Cooled RF Coil for High-Resolution In Vivo Imaging on a 3-Tesla Whole-Body Scanner. IEEE Trans. Instrum. Meas. 2012;61:129–139 doi: 10.1109/TIM.2011.2157575.

14. Ardenkjaer-Larsen JH, Fridlund B, Gram A, et al. Increase in signal-to-noise ratio of > 10,000 times in liquid-state NMR. Proc. Natl. Acad. Sci. 2003;100:10158–10163 doi: 10.1073/pnas.1733835100.

15. Reykowski A, Wright SM, Porter JR. Design of Matching Networks for Low Noise Preamplifiers. MRM 1995:848–852.

16. Sanchez-Heredia JD, Szocska Hansen ES, Laustsen C, Zhurbenko V, Ardenkjær-Larsen JH. Low-Noise Active Decoupling Circuit and its Application to 13C Cryogenic RF Coils at 3T. TOMOGRAPHY 2017;3:60:66 doi: 10.18383/j.tom.2016.00280.

17. Josan S, Hurd R, Billingsley K, et al. Effects of isoflurane anesthesia on hyperpolarized ^{13} C metabolic measurements in rat brain. Magn. Reson. Med. 2013;70:1117–1124 doi: 10.1002/mrm.24532.

18. Miller JJ, Grist JT, Serres S, et al. 13C Pyruvate Transport Across the Blood-Brain Barrier in Preclinical Hyperpolarised MRI. Sci. Rep. 2018;8:15082 doi: 10.1038/s41598-018-33363-5.

19. Johnson JB. Thermal Agitation of Electricity in Conductors. Phys. Rev. 1928;32:97–109 doi: 10.1103/PhysRev.32.97.

For Peer Review

20. Jerosch-Herold M, Kirschman RK. Potential benefits of a cryogenically cooled NMR probe for room-temperature samples. J. Magn. Reson. 1989;85:141–146 doi: 10.1016/0022-2364(89)90327-2.

21. Matula RA. Electrical resistivity of copper, gold, palladium, and silver. J. Phys. Chem. Ref. Data 1979;8:1147 doi: 10.1063/1.555614.

22. Nemoto T, Sasaki S, Hakuraku Y. Thermal conductivity of alumina and silicon carbide ceramics at low temperatures. Cryogenics (Guildf). 1985;25:531–532 doi: 10.1016/0011-2275(85)90080-3.

23. Kumar A, Edelstein WA, Bottomley PA. Noise figure limits for circular loop MR coils. Magn. Reson. Med. 2009;61:1201–1209 doi: 10.1002/mrm.21948.

24. Gabriel C. Compilation of the Dielectric Properties of Body Tissues at RF and Microwave Frequencies. DTIC Document; 1996.

25. Mispelter J, Lupu M, Briguet A. NMR Probeheads for Biophysical and Biomedical Experiments: Theoretical Principles & Practical Guidelines. Imperial College Press; 2006.

26. Constantinides CD, Atalar E, McVeigh ER. Signal-to-noise measurements in magnitude images from NMR phased arrays. Magn. Reson. Med. 1997;38:852–857 doi: 10.1002/mrm.1910380524.

27. Derby K, Tropp J, Hawryszko C. Design and evaluation of a novel dual-tuned resonator for spectroscopic imaging. J. Magn. Reson. 1990;86:645–651 doi: 10.1016/0022-2364(90)90043-9.

28. Tropp J, Lupo JM, Chen A, et al. Multi-channel metabolic imaging, with SENSE reconstruction, of hyperpolarized [1-13C] pyruvate in a live rat at 3.0tesla on a clinical MR scanner. J. Magn. Reson. 2011;208:171–177 doi: 10.1016/j.jmr.2010.10.007.

29. Nelson SJ, Kurhanewicz J, Vigneron DB, et al. Metabolic Imaging of Patients with Prostate Cancer Using Hyperpolarized [1-13C]Pyruvate. Sci. Transl. Med. 2013;5:198ra108–198ra108 doi: 10.1126/scitranslmed.3006070.

30. Schulte RF, Sperl JI, Weidl E, et al. Saturation-recovery metabolic-exchange rate imaging with hyperpolarized [1- ^{13} C] pyruvate using spectral-spatial excitation. Magn. Reson. Med. 2013;69:1209–1216 doi: 10.1002/mrm.24353.

31. Ardenkjaer-Larsen JH, Leach AM, Clarke N, Urbahn J, Anderson D, Skloss TW. Dynamic nuclear polarization polarizer for sterile use intent. NMR Biomed. 2011;24:927–932 doi: 10.1002/nbm.1682.

32. Qi H, Nielsen PM, Schroeder M, Bertelsen LB, Palm F, Laustsen C. Acute renal metabolic effect of metformin assessed with hyperpolarised MRI in rats. Diabetologia 2018;61:445–454 doi: 10.1007/s00125-017-4445-6.

33. Wright AC, Song HK, Wehrli FW. In vivo MR micro imaging with conventional radiofrequency coils cooled to 77K. Magn. Reson. Med. 2000;43:163–169 doi: 10.1002/(SICI)1522-2594(200002)43:2<163::AID-MRM1>3.0.CO;2-K.

34. McCulloch MA, Grahn J, Melhuish SJ, et al. Dependence of noise temperature on physical temperature for cryogenic low-noise amplifiers. J. Astron. Telesc. Instruments, Syst. 2017;3:014003 doi: 10.1117/1.JATIS.3.1.014003.

35. Roemer PB, Edelstein WA, Hayes CE. The NMR Phased Array. MRM 1990;225:192–225.

36. Arunachalam A, Whitt D, Fish K, et al. Accelerated spectroscopic imaging of hyperpolarized C-13 pyruvate using SENSE parallel imaging. NMR Biomed. 2009;22:867–873 doi: 10.1002/nbm.1401.

For Peer Review

For Peer Review

List of Figure Captions

Figure 1. Schematic of the proposed cryostat: the LN_2 flows from the reservoir (on the right), to the vacuum-insulated cylindrical vessel (on the left). The vessel is thermally connected to a cold-finger made of Al_2O_3, which has the RF coil attached (showed in orange color in the figure). Dimensions are shown in mm.

Figure 2. a) Fabricated cryostat and b) detail of the cold-finger with the receive RF coil attached.

Figure 3. In-vivo experiments setup: the animal is placed in belly-up position to minimize the coil-to-brain distance, since the cryogenic coil is placed at the bottom part of the cryostat bore.

Figure 4. Measured performance of the cryogenic coil over time. The bold line shows the performance when the cryostat is filled with 6 liters of LN_2 (basic use), while the dotted line includes a refilling of 4 liters of LN_2 after 4 hours (extended use). After 45 min of cooling, the coil is fully cold and stable, and can be disconnected from the vacuum pump and place inside the MRI scanner. The thermal insulation last for the next 12 h in the basic use (15 h in the extended use), after which the cryostat vacuum needs to be rebuilt.

Figure 5. Measured temperature of the animal and coil positions at the cryostat over time, with and without applying warm air through the inner bore. Warm air was applied first for 5 min (min 70 to 75) and later for 50 min (min 100 to 150).

Figure 6. Measured SNR over the entire FOV (80x80x10 mm) for the different coil setups: a) Room temperature surface coil placed at 3 mm from the sample, b) Room temperature surface coil placed as close as possible to the phantom, c) Cryogenic surface coil, and d) Room temperature volume coil. The two different surface coils used at 290 K and 88 K are identical in size and shape.

Figure 7. In-vivo experiment #1: 2D-localized dynamic 13C spectroscopic data, over a sagittal slice centered at the brain. The different detected metabolites are shown from left to right, while the metabolic dynamics of the experiment are shown from top to bottom. Each of the metabolic maps shown are normalized to their respective maximum.

Figure 8. In-vivo experiment #2: 2D-localized dynamic 13C spectroscopic data, over a coronal slice centered at the brain. The different detected metabolites are shown from left to right, while the metabolic dynamics of the experiment are shown from top to bottom. Each of the metabolic maps shown are normalized to their respective maximum.

Supporting Information Figure S1. Coil positioning for the Q-factor measurements used to characterize the loading of the phantom used for imaging: a) Bicarbonate phantom, b) Rat head, and c) Rat abdomen. The images show the case with coil-to-sample distance = 0 mm, and measurements were repeated with a coil-to-sample distance of 3 mm (replicating the coil-to-sample distance of the cryostat).

For Peer Review

List of Table Captions

Table 1. Measured Q-Factors.

Table 2. WMA32C preamplifier characterization.

Supporting Information Table S1. Measured Q-factors at Room Temperature.

For Peer Review

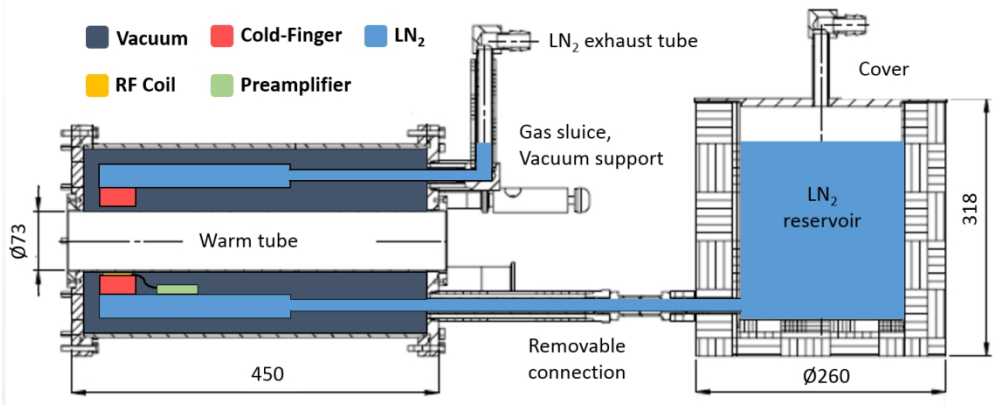

Figure 1. Schematic of the proposed cryostat: the LN2 flows from the reservoir (on the right), to the vacuum-insulated cylindrical vessel (on the left). The vessel is thermally connected to a cold-finger made of Al2O3, which has the RF coil attached (showed in orange color in the figure). Dimensions are shown in mm.

122x49mm (300 x 300 DPI)

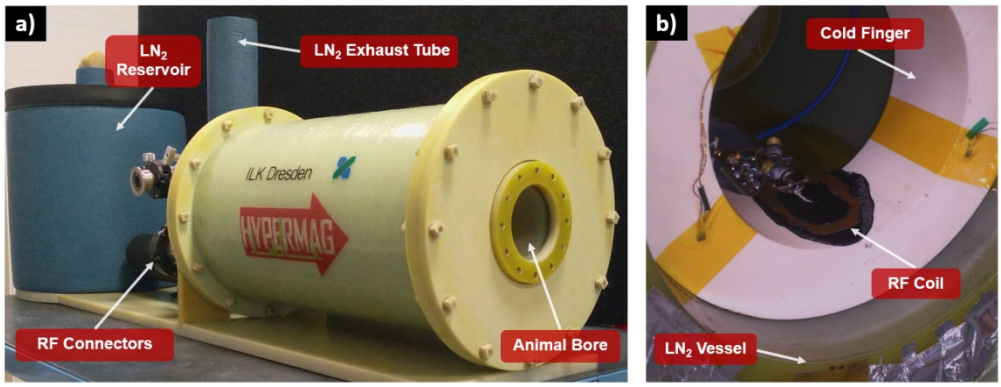

Figure 2. a) Fabricated cryostat and b) detail of the cold-finger with the receive RF coil attached.

124x47mm (300 x 300 DPI)

Figure 3. In-vivo experiments setup: the animal is placed in belly-up position to minimize the coil-to-brain distance, since the cryogenic coil is placed at the bottom part of the cryostat bore.

111x77mm (300 x 300 DPI)

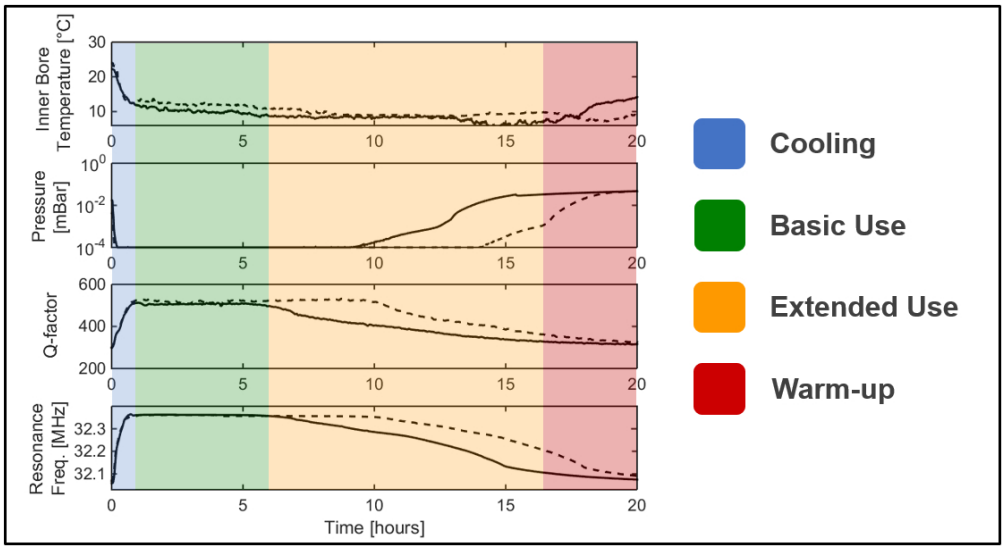

Figure 4. Measured performance of the cryogenic coil over time. The bold line shows the performance when the cryostat is filled with 6 liters of LN2 (basic use), while the dotted line includes a refilling of 4 liters of LN2 after 4 hours (extended use). After 45 min of cooling, the coil is fully cold and stable, and can be disconnected from the vacuum pump and place inside the MRI scanner. The thermal insulation last for the next 12 h in the basic use (15 h in the extended use), after which the cryostat vacuum needs to be rebuilt.

94x51mm (300 x 300 DPI)

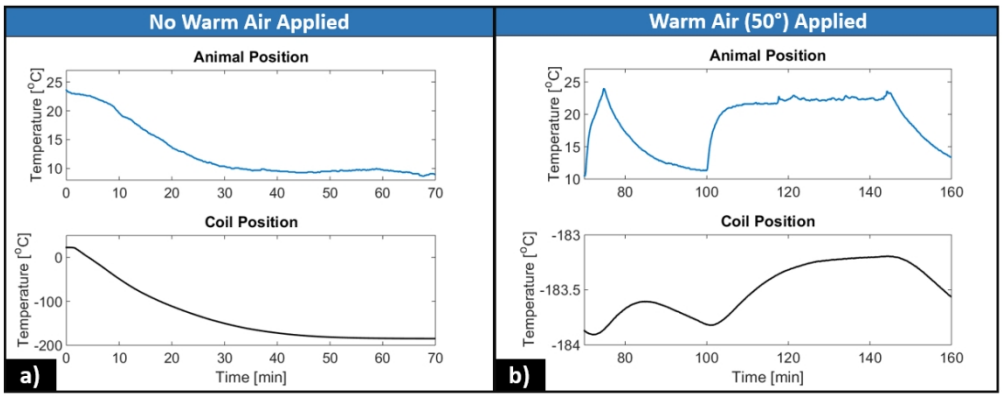

Figure 5. Measured temperature of the animal and coil positions at the cryostat over time, with and without applying warm air through the inner bore. Warm air was applied first for 5 min (min 70 to 75) and later for 50 min (min 100 to 150).

104x41mm (300 x 300 DPI)

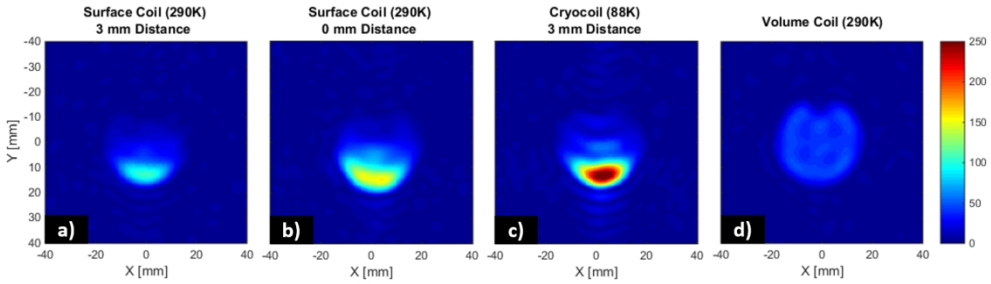

Figure 6. Measured SNR over the entire FOV (80x80x10 mm) for the different coil setups: a) Room temperature surface coil placed at 3 mm from the sample, b) Room temperature surface coil placed as close as possible to the phantom, c) Cryogenic surface coil, and d) Room temperature volume coil. The two different surface coils used at 290 K and 88 K are identical in size and shape.

142x41mm (300 x 300 DPI)

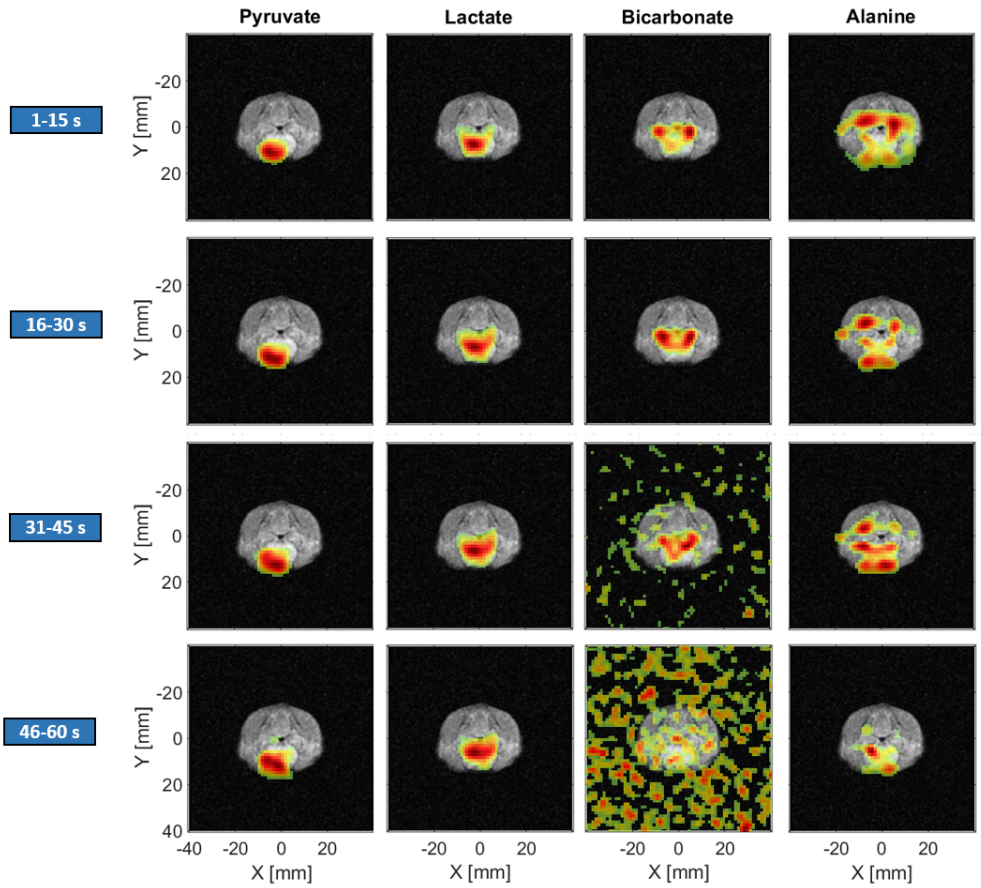

Figure 7. In-vivo experiment #1: 2D-localized dynamic 13C spectroscopic data, over a sagittal slice centered at the brain. The different detected metabolites are shown from left to right, while the metabolic dynamics of the experiment are shown from top to bottom. Each of the metabolic maps shown are normalized to their respective maximum.

90x80mm (300 x 300 DPI)

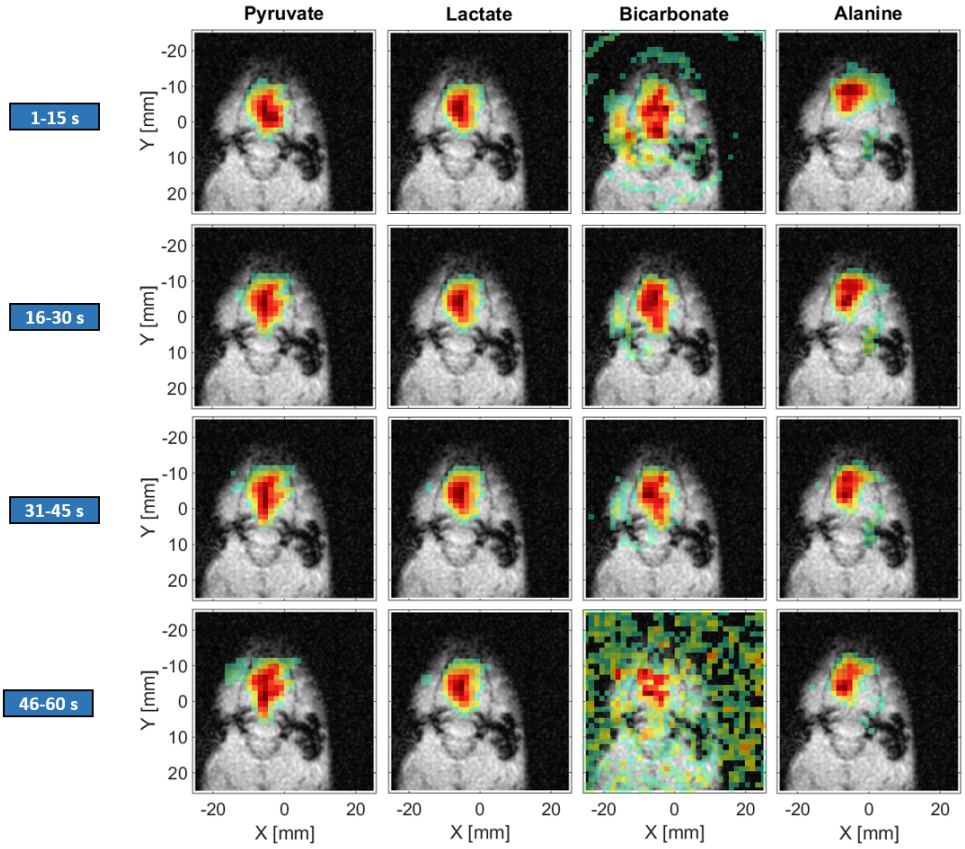

Figure 8. In-vivo experiment #2: 2D-localized dynamic 13C spectroscopic data, over a coronal slice centered at the brain. The different detected metabolites are shown from left to right, while the metabolic dynamics of the experiment are shown from top to bottom. Each of the metabolic maps shown are normalized to their respective maximum.

94x80mm (300 x 300 DPI)

TABLE I
MEASURED Q-FACTORS.

	Free Space		Cryostat	
	290K	77K	290K	88K
Q_{UN}	280	590	280	550
Q_{LO}	245	-	245	430

Q_{UN} = non sample-loaded Q-factor, Q_{LO} = sample-loaded Q-factor

For Peer Review

TABLE II
WMA32C PREAMPLIFIER CHARACTERIZATION.

	290K	77K
NF [dB]	0.7	0.25
T_{eq} [K]	51	17
Gain [dB]	28.2	22.5
I [mA]	16	11

For Peer Review

Supporting Information

Supporting Information Figure S1. Coil positioning for the Q-factor measurements used to characterize the loading of the phantom used for imaging: a) Bicarbonate phantom, b) Rat head, and c) Rat abdomen. The images show the case with coil-to-sample distance = 0 mm, and measurements were repeated with a coil-to-sample distance of 3 mm (replicating the coil-to-sample distance of the cryostat).

SUPPORTING INFORMATION TABLE S1
MEASURED Q-FACTORS AT ROOM TEMPERATURE.

	0 mm	3 mm
Unloaded	280	
Loaded (Phantom)	170	245
Loaded (Rat Head)	220	263
Loaded (Rat Abdomen)	193	223

For Review